Downloaded from UvA-DARE, the institutional repository of the University of Amsterdam (UvA) http://hdl.handle.net/11245/2.17165

File ID uvapub:17165 Filename 96202y.pdf Version unknown

# SOURCE (OR PART OF THE FOLLOWING SOURCE):

Type article

Title Spectral Evolution of Circinus X-1 along Its Orbit

Author(s) R. Iaria, T. di Salvo, L. Burderi, N.R. Robba

Faculty FNWI: Astronomical Institute Anton Pannekoek (IAP)

Year 2001

## FULL BIBLIOGRAPHIC DETAILS:

http://hdl.handle.net/11245/1.187272

## Copyright

It is not permitted to download or to forward/distribute the text or part of it without the consent of the author(s) and/or copyright holder(s), other than for strictly personal, individual use, unless the work is under an open content licence (like Creative Commons).

# SPECTRAL EVOLUTION OF CIRCINUS X-1 ALONG ITS ORBIT

R. IARIA, T. DI SALVO, L. BURDERI, AND N. R. ROBBA Received 2001 March 30; accepted 2001 July 9

#### **ABSTRACT**

We report on the spectral analysis of Circinus X-1 observed by the ASCA satellite in 1998 March along one orbital period. The luminosity of the source (in the 0.1–100 keV band) ranges from  $2.5 \times 10^{38}$  ergs s<sup>-1</sup> at the periastron (orbital phase 0.01) to  $1.5 \times 10^{38}$  ergs s<sup>-1</sup> at orbital phase 0.3. From the spectral analysis and the light curve, we argue that Cir X-1 shows three states along the orbital evolution. The first state is at the orbital phase interval 0.97–0.3: the luminosity becomes super-Eddington, and a strong flaring activity is present. In this state a shock could form in the inner region of the system because of the super-Eddington accretion rate, producing an outflow of ionized matter whose observational signature could be the prominent absorption edge at ~8.7 keV observed in the energy spectrum at these phases. In the second state, corresponding to the orbital phase interval between 0.3 and 0.7, the accretion rate is sub-Eddington, and we observe a weaker outflow, with a smaller hydrogen column: the absorption edge is now at ~8.3 keV with an optical depth a factor of 2.5–6 smaller. The third state corresponds to the orbital phase interval 0.78–0.97. In this state the best-fit model to the spectrum requires the presence of a partial covering component, indicating that the emission from the compact object is partially absorbed by neutral matter, probably the atmosphere of the companion star and/or the accreting matter from the companion.

Subject headings: binaries: close — stars: individual (Circinus X-1) — stars: neutron — X-rays: individual (Circinus X-1) — X-rays: stars

#### 1. INTRODUCTION

Circinus X-1 is a puzzling X-ray binary. Because of its rapid variability, a black hole was supposed to be the compact object in this system (Toor 1977) until type I X-ray bursts were detected (Tennant, Fabian, & Shafer 1986a, 1986b), suggesting that the compact object is a neutron star. A modulation with a period of 16.6 days was observed at several wavelengths in the emission of the source. The high stability of this period was a strong indication that it is the orbital period of Cir X-1. The orbit is highly eccentric  $(e \sim 0.9)$ ; Murdin et al. 1980; Tauris et al. 1999). Periodic radio flares near the zero phase (i.e., at the periastron; for recent ephemeris, see Stewart et al. 1991) are also accompanied by drastic changes in the X-ray light curve (X-ray flares and dips). The position of the probable radio counterpart is close to the supernova remnant G321.9-0.3 (Clark, Parkinson, & Caswell 1975), suggesting that Cir X-1 could be a runaway binary. Case & Bhattacharya (1998) have revised the distance to the supernova remnant G321.9-0.3, and hence to the associated Cir X-1, to 5.5 kpc. Therefore, in the following discussion we adopt 5.5 kpc as the distance to the

Quasi-periodic oscillations (QPOs) at 100–200 Hz were observed in this source (Tennant 1987; Shirey et al. 1996), but no kilohertz QPOs were detected. Recently, Iaria et al. (2001) detected the presence of highly ionized matter around Cir X-1, with a hydrogen column density of  $\sim 10^{24}$  cm $^{-2}$  at the orbital phase interval 0.11–0.16. The continuum emission was fitted using a Comptonization model

plus a power-law tail at energies higher than 10 keV. The luminosity of the power law is 4% of the total. Brandt & Schulz (2000), analyzing Chandra observations taken at the periastron, detected, for the first time in the X-ray band, the presence of P Cygni lines in X-ray band. They explain these features as being caused by the presence of high-velocity outflows from this system (probably a moderatetemperature, ~0.5 keV wind from the X-ray-heated accretion disk). Johnston, Fender, & Wu (1999), using several infrared (IR) and optical data from 1976 to 1997, observed an asymmetric  $H\alpha$  emission line along the whole orbit. They argued that the broad component of the emission line arises in a high-velocity ( $\sim 2000 \text{ km s}^{-1}$ ), optically thick flow near the neutron star. Brandt et al. (1996), using ASCA data taken during 1994 August 4-5, found a sudden variation of the flux at the periastron phase, the count rate increasing from  $\sim 30$  to  $\sim 300$  counts s<sup>-1</sup>. In the low count rate state they obtained a good fit using a partial covering component, in addition to a two-blackbody model, with a corresponding hydrogen column of  $\sim 10^{24}$  cm<sup>-2</sup>; in the high count rate state the partial covering of the X-ray spectrum was not needed. Because of the similarity to the spectra of Seyfert 2 galaxies with Compton-thin tori, Brandt et al. (1996) suggested that matter at the outer edge of the accretion disk together with an edge-on disk orientation could explain the partial covering of the spectrum in Cir X-1.

Here we report the results of the spectral analysis in the energy range 0.6–10 keV performed on Cir X-1 data from the *ASCA* satellite taken in 1998. These data cover a whole orbital period, allowing us to study the corresponding changes in the properties of the matter around the system.

#### 2. OBSERVATIONS AND LIGHT CURVE

We performed a systematic spectral study of Cir X-1 along its orbital period using ASCA archival data taken between 1998 March 3 and 18. The instruments on board ASCA (Tanaka, Inoue, & Holt 1994) consist of two Solid-

<sup>&</sup>lt;sup>1</sup> Dipartimento di Scienze Fisiche ed Astronomiche, Università di Palermo, via Archirafi n.36, 90123 Palermo, Italy; iaria@gifco.fisica.unipa.it.

<sup>&</sup>lt;sup>2</sup> Astronomical Institute "Anton Pannekoek," and Center for High-Energy Astrophysics, University of Amsterdam, Kruislaan 403, NL 1098 SJ Amsterdam, Netherlands.

<sup>&</sup>lt;sup>3</sup> Osservatorio Astronomico di Roma, via Frascati 33, 00040 Monteporzio Catone, Roma, Italy.

State Imaging Spectrometers (SISs) and two Gas Imaging Spectrometers (GISs; Ohashi et al. 1996; Makishima et al. 1996). In our analysis we used only data from GIS instruments. GISs have an energy resolution of  $\sim 8\%$  (FWHM) at 6 keV, and their detection efficiency above  $\sim$  3 keV is higher than that of the SISs (it is twice as large as the SIS detection efficiency at energies of 6.5-7 keV). We used data at high telemetry from the ASCA archive, screened using current standard filter criteria. The GIS photon extraction region was limited to the standard circular region of 6' radius centered on the source. The background was taken from a 6' radius circle free of emission from Cir X-1 in the external region of the GIS field of view and after an accurate investigation of the uniform background distribution. Because of the high luminosity of the source, it was necessary to add a dead-time correction after the extraction of the light curves and the spectra. To correct for this effect, we used the FTOOLs tasks ldeadtime and deadtime for light curves and spectra, respectively, using the corresponding mkf files (which contain the time histories of various parameters from which good data can be identified and screened) for each observation. A systematic error of 2% was added to the spectra. The observations used for the analysis cover an entire orbital period from 1998 March 3 to 19. In Table 1 we report for each of the seven analyzed observations (labeled A-G) the start and stop times, the exposure time, and the relative orbital phase, assuming the orbital ephemeris as reported by Stewart et al. (1991).

In Figure 1 we plot the Cir X-1 light curve in the energy band 0.6-10 keV (top) and the corresponding hardness ratio, i.e., the ratio of the count rate in the energy band 3-7 keV to that in the band 1-3 keV (bottom). Large variabilities are observed in the light curve, especially at the orbital phase interval 0-0.2, where sudden flux variations are visible, with the count rate ranging from  $\sim 400$  to  $\sim 600$ counts s<sup>-1</sup>. In the same phase interval we observe a rapid decrease of the hardness ratio from  $\sim 0.95$  to  $\sim 0.4$ . In the phase interval 0.3-0.6, the light curve does not show any significant variability and the count rate is  $\sim 300$  counts s<sup>-1</sup>, while the hardness ratio increases from 0.7 to 0.9. In the phase interval 0.75-0.88 the light curve shows a count rate slightly higher than 200 counts s<sup>-1</sup>, and the hardness ratio is constant at  $\sim 1.05$ . The longest observation on March 3 shows a large variability in the hardness ratio. Therefore, we divided this observation into four intervals (labeled A1, A2, A3, and A4), the first corresponding to the orbital phase 0.95, the second to 0.98-1, the third to 0.01-0.04, and the fourth to 0.05-0.09. In Table 2 we report the intervals in which the light curve was divided and the corresponding orbital phases. We also show for each of the intervals the flux of the source extrapolated in the 2.5-25 keV energy range in order to compare these values with previous observations. The flux in the 2.5-25 keV band is very similar to that measured by Shirey et al. (1999) with the Rossi X-Ray Timing Explorer (RXTE) satellite. In the same table we also report the flux of the source extrapolated in the 0.1–100 keV

 $\begin{tabular}{ll} TABLE & 1 \\ Log of Used & ASCA & Observations \\ \end{tabular}$ 

Observation	Start Time (UTC)	Stop Time (UTC)	Exposure Time (ks)	Orbital Phase
A	1998 Mar 3 (12:12:49)	1998 Mar 5 (18:50:33)	38.2	0-0.09, 0.95-1
В	1998 Mar 6 (23:33:13)	1998 Mar 7 (09:00:43)	7.9	0.17-0.19
C	1998 Mar 9 (04:19:38)	1998 Mar 9 (15:10:39)	10.2	0.30-0.33
D	1998 Mar 11 (02:21:16)	1998 Mar 11 (13:30:52)	6.9	0.41 - 0.44
E	1998 Mar 13 (02:12:29)	1998 Mar 13 (13:20:47)	8.4	0.54-0.56
F	1998 Mar 17 (00:44:30)	1998 Mar 17 (11:20:24)	4.9	0.78 - 0.80
G	1998 Mar 18 (16:24:23)	1998 Mar 19 (00:21:19)	3.9	0.87-0.89

Note.—For each of the analyzed observations, we show the start and stop times (in Universal Time, second and third columns), the exposure time not corrected for the dead time (fourth column), and the corresponding orbital phases (fifth column), referred to the ephemeris obtained by Stewart et al. (1991).

 ${\bf TABLE~2}$  Spectral Features, Flux, and Luminosity in the Selected Intervals

Interval	Absorption Edge	Partial Covering	Emission Line	Flux (2.5–25 keV)	Flux (0.1–100 keV)	Luminosity (0.1–100 keV)	Orbital Phase
A1	No	Yes	No	3.8	5.8	2.1	0.95
A2	No	No	Yes	3.8	5.4	1.9	0.99
A3	No	No	Yes	4.1	7.0	2.5	0.01 - 0.04
A4	Yes	No	Yes	2.5	5.9	2.1	0.05-0.09
В	Yes	No	No	2.8	6.4	2.3	0.17-0.19
C	Yes	No	Yes	2.4	4.3	1.5	0.30 - 0.33
D	Yes	No	Yes	2.7	4.6	1.6	0.41 - 0.44
E	Yes	No	Yes	2.7	4.3	1.6	0.54-0.56
F	No	Yes	No	3.1	4.6	1.7	0.78 - 0.80
G	No	Yes	No	3.5	5.0	1.8	0.87-0.89

Note.—For each of the intervals we report the spectral features that were necessary to fit the corresponding spectra in addition to the Comptonization model. We also report the flux, in units of  $10^{-8}$  ergs cm<sup>-2</sup> s<sup>-1</sup>, and the luminosity, in units of  $10^{38}$  ergs s<sup>-1</sup>, assuming a distance to the source of 5.5 kpc (Case & Bhattacharya 1998) calculated in the indicated energy ranges.

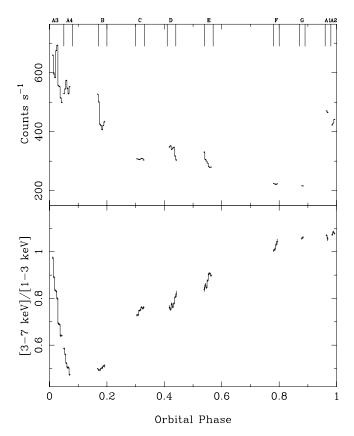


FIG. 1.—Top: Cir X-1 light curve in the energy band 0.6–10 keV. The intervals into which we divided these observations are also indicated with the corresponding labels. *Bottom*: Ratio of the count rate in the energy band 3–7 keV to that in the 1–3 keV band. The bin time is 5595 s.

energy range (using the best-fit spectral model discussed in the next section) and the corresponding luminosity of the source.

## 3. SPECTRAL ANALYSIS

For each of the 10 intervals described above, corresponding to different orbital phases, we extracted energy spectra in the 0.6–10 keV band in order to study the spectral variations along the orbit. The continuum emission was fitted using a Comptonization model (COMPTT; Titarchuk 1994) modified at low energies by photoelectric absorption by cold matter. In a previous paper (Iaria et al. 2001), the broadband (0.1-100 keV) spectrum from the BeppoSAX satellite did not allow us to distinguish between a simple Comptonization and the so-called Eastern model, consisting of a multicolor disk blackbody plus a blackbody component (Mitsuda et al. 1984). However, because of the large value of the neutron star radius obtained from the fit ( $\sim 35$ km), we preferred the Comptonization model to fit the spectrum. Therefore, we use the same model here. The average photoelectric absorption obtained from the fit is  $\sim 1.6 \times 10^{22}$  cm<sup>-2</sup>. The seed photon temperature varies from 0.51 keV near the periastron to 0.37 keV at orbital phase 0.89. The electron temperature varies from 1 keV (at orbital phase  $\sim 0.2$ ) up to 1.7 keV (at orbital phase 0.89). The Compton optical depth varies between 16 and 20 along the orbital period.

In spectra A1, F, and G we improved the fit, adding a partial covering to the model. The probability of chance improvement for the addition of this component, estimated using an F-test, was 0.08,  $2.8 \times 10^{-10}$ , and  $5.3 \times 10^{-5}$ , respectively. Note that this component is essentially needed

 $\label{eq:table 3} TABLE \ 3$  Results of the Fit of Cir X-1 for the First Five Spectra

Spectra Orbital Phase	A1 (0.95)	A2 (0.99)	A3 (0.01–0.04)	A4 (0.05–0.09)	B (0.17–0.19)	
$N_{\rm H}  (\times 10^{22}  {\rm cm}^{-2}) \dots$	1.630 (fixed)	$1.630^{+0.030}_{-0.033}$	$1.6800^{+0.0094}_{-0.0078}$	1.5400+0.0084	$1.627^{+0.011}_{-0.007}$	
$N_{\rm H_{PC}} \ (\times 10^{23} \ {\rm cm^{-2}}) \dots$	$1.00^{+0.29}_{-0.46}$		•••	•••		
f	$0.21^{+0.12}_{-0.17}$					
E <sub>edge</sub> (keV)	•••	8.3 (fixed)	8.3 (fixed)	$8.464^{+0.102}_{-0.097}$	$8.71^{+0.15}_{-0.16}$	
$ au_{ ext{edge}}$		< 0.0094	< 0.037	$0.353 \pm 0.065$	$0.381 \pm 0.098$	
$kT_0$ (keV)	$0.507 \pm 0.033$	$0.519^{+0.020}_{-0.007}$	$0.4860^{+0.0025}_{-0.0020}$	$0.4480 \pm 0.0017$	$0.4403^{+0.0025}_{-0.0018}$	
$kT_e$ (keV)	$1.556^{+0.136}_{-0.087}$	$1.491^{+0.028}_{-0.011}$	$1.2660^{+0.0030}_{-0.0019}$	$1.0720^{+0.0026}_{-0.0016}$	$1.1210 \pm 0.0027$	
τ	$17.4 \pm 3.0$	$20.07^{+0.23}_{-0.65}$	$18.570^{+0.063}_{-0.048}$	$16.120^{+0.055}_{-0.058}$	$16.380^{+0.061}_{-0.099}$	
$N_{ m comp}$	$11.48^{+0.82}_{-1.17}$	$10.91^{+0.18}_{-0.33}$	$20.890^{+0.052}_{-0.119}$	$27.020^{+0.094}_{-0.072}$	$26.800^{+0.080}_{-0.123}$	
$f_{\text{bol}} (\times 10^{-8}) \dots$	5.8	5.4	7.0	5.9	6.4	
$R_{\mathbf{W}}$ (km)	$71 \pm 10$	$59.6 \pm 4.9$	$87.8 \pm 1.2$	$112.3 \pm 1.3$	$117.5 \pm 1.4$	
$E_{\rm Fe}$ (keV)		$6.616^{+0.038}_{-0.108}$	$6.726 \pm 0.052$	$6.731 \pm 0.068$		
$\sigma_{\rm Fe}$ (keV)		< 0.17	$0.174^{+0.069}_{-0.072}$	< 0.15		
$I_{\rm Fe}  (\times 10^{-2}) \dots$		$1.01^{+0.33}_{-0.24}$	$1.84^{+0.31}_{-0.26}$	$0.61^{+0.13}_{-0.12}$		
EW <sub>Fe</sub> (eV)		$33.2^{+10.8}_{-7.9}$	$74.5^{+12.4}_{-10.6}$	$67.0^{+14.7}_{-12.9}$		
$\chi^2$ /degrees of freedom	309/391	252/389	244/389	259/387	263/390	
F-test (line)	•••	$2.1 \times 10^{-28}$	~0	~0	•••	
F-test (edge)		~1	~1	~0	$4.17 \times 10^{-28}$	
F-test (PC)	0.08	•••				

Note.—The continuum model consists of a Comptonized spectrum modeled by COMPTT. Uncertainties are at a 90% confidence level for a single parameter.  $N_{\rm Hrc}$  is the hydrogen column corresponding to the partial covering, f is the fraction of covered area by the neutral matter,  $kT_0$  is the temperature of the seed photons for the Comptonization,  $kT_e$  is the electron temperature,  $\tau$  is the optical depth of the scattering cloud using a spherical geometry,  $R_{\rm W}$  is the radius of the seed photon Wien spectrum in kilometers, and  $f_{\rm bol}$  is the intrinsic flux of the Comptonized component in units of ergs cm $^{-2}$  s $^{-1}$ . EW $_{\rm Fe}$  is the equivalent width of the Gaussian emission line,  $E_{\rm Fe}$  the centroid energy of the line, and  $I_{\rm Fe}$  is the intensity of the emission line in units of photons cm $^{-2}$  s $^{-1}$ . "F-test" indicates the probability of the chance improvement of the fit when the feature indicated in parentheses is included in the spectral model.

TABLE 4
RESULTS OF THE FIT OF CIR X-1 FOR THE LAST FIVE SPECTRA

Spectra Orbital Phase	C (0.30–0.33)	D (0.41-0.44)	E (0.54–0.56)	F (0.78-0.80)	G (0.87–0.89)
$N_{\rm H}  (\times 10^{22}  {\rm cm}^{-2}) \dots$	$1.542^{+0.046}_{-0.017}$	$1.629^{+0.035}_{-0.068}$	$1.628 \pm 0.054$	$1.619 \pm 0.080$	$1.659^{+0.080}_{-0.097}$
$N_{\rm H_{PC}}  (\times 10^{23}  {\rm cm}^{-2}) \dots$	•••	•••		$6.9^{+3.6}_{-2.4}$	$10.8^{+8.4}_{-6.8}$
f		•••		$0.207^{+0.106}_{-0.067}$	$0.25^{+0.66}_{-0.15}$
$E_{\text{edge}}$ (keV)	$8.23 \pm 0.11$	8.3 (fixed)	$8.34^{+0.31}_{-0.27}$	•••	•••
τ <sub>edge</sub>	$0.151^{+0.030}_{-0.039}$	< 0.075	$0.062^{+0.046}_{-0.033}$		•••
$kT_0$ (keV)	$0.396^{+0.013}_{-0.016}$	$0.416^{+0.026}_{-0.011}$	$0.391 \pm 0.020$	$0.383^{+0.029}_{-0.034}$	$0.369^{+0.041}_{-0.017}$
$kT_e$ (keV)	$1.280^{+0.022}_{-0.018}$	$1.354^{+0.027}_{-0.011}$	$1.505^{+0.032}_{-0.018}$	$1.699^{+0.013}_{-0.035}$	$1.762^{+0.031}_{-0.034}$
τ	$20.92^{+0.33}_{-0.48}$	$19.48^{+0.25}_{-0.60}$	$19.94^{+0.29}_{-0.48}$	$20.17^{+0.54}_{-0.41}$	$20.16^{+0.45}_{-0.32}$
$N_{ ext{comp}}$	$12.29 \pm 0.37$	$12.28^{+0.26}_{-0.72}$	$9.46^{+0.31}_{-0.47}$	$7.80 \pm 0.78$	$8.1^{+4.6}_{-1.7}$
$f_{\text{bol}} (\times 10^{-8}) \dots$	4.3	4.6	4.3	4.6	5.0
$R_{\mathbf{W}}$ (km)	$93 \pm 8$	91 ± 12	94 ± 10	95 ± 17	$106 \pm 23$
$E_{\mathbf{Fe}}$ (keV)	$6.759^{+0.074}_{-0.064}$	$6.811^{+0.095}_{-0.100}$	$6.763 \pm 0.099$	•••	•••
$\sigma_{\rm Fe}$ (keV)	$0.196^{+0.122}_{-0.077}$	$0.25 \pm 0.16$	$0.27^{+0.16}_{-0.19}$	•••	•••
$I_{\rm Fe}  (\times 10^{-2}) \dots \dots$	$1.05^{+0.33}_{-0.20}$	$1.16^{+0.43}_{-0.37}$	$1.12^{+0.43}_{-0.46}$	•••	•••
$\mathrm{EW}_{\mathrm{Fe}}\left(\mathrm{eV}\right)\dots$	$63.0^{+19.5}_{-12.2}$	$70.7^{+26.5}_{-22.4}$	$50.9^{+19.7}_{-20.8}$	•••	•••
$\chi^2$ /degrees of freedom	256/387	251/387	250/387	285/390	309/390
F-test (line)	~0	$3.6 \times 10^{-38}$	$8.0 \times 10^{-10}$		•••
F-test (edge)	$1.2 \times 10^{-7}$	~1	$6.2 \times 10^{-22}$	•••	•••
F-test (PC)	•••	•••	•••	$2.8 \times 10^{-10}$	$5.3 \times 10^{-5}$

Note.—The continuum model consists of a Comptonized spectrum modeled by COMPTT. Uncertainties are at a 90% confidence level for a single parameter.  $N_{\rm H_{PC}}$  is the hydrogen column corresponding to the partial covering, f is the fraction of covered area by the neutral matter,  $kT_0$  is the temperature of the seed photons for the Comptonization,  $kT_e$  is the electron temperature,  $\tau$  is the optical depth of the scattering cloud using a spherical geometry,  $R_{\rm W}$  is the radius of the seed photon Wien spectrum in kilometers, and  $f_{\rm bol}$  is the intrinsic flux of the Comptonized component in units of ergs cm $^{-2}$  s $^{-1}$ . EW $_{\rm Fe}$  is the equivalent width of the Gaussian emission line,  $E_{\rm Fe}$  the centroid energy of the line, and  $I_{\rm Fe}$  is the intensity of the emission line in units of photons cm $^{-2}$  s $^{-1}$ . "F-test" indicates the probability of the chance improvement of the fit when the feature indicated in parentheses is included in the spectral model.

to fit an iron absorption edge. In fact, we obtain equivalently good fits if we use an absorption edge at energies between 7.6 and 7.9 keV instead of the partial covering for these intervals. In this case, the edge optical depth ranges from 0.008 for interval A1 to 0.12 for interval F. However, in agreement with the results of Brandt et al. (1996), in the following we adopt and discuss the partial covering interpretation.

In some spectra (A4 to E) we detected the presence of an absorption edge from highly ionized iron. In the spectra where the partial covering is present, there is no evidence of a such feature. In A2, A3, and D neither the partial covering nor the absorption edge is present; in these cases we could only find an upper limit on the optical depth of the absorption edge. An emission line from ionized iron is also needed to fit some of the spectra (A2 to A4 and C to E). In Table 2 we show the spectral features that were included in the best-fit model for each of the 10 spectra, and in Tables 3 and 4 we report the parameters of the best-fit model, together with the probability of chance improvement of the fit when the indicated component is included in the spectral model.

#### 4. DISCUSSION

We analyzed data of Cir X-1 from seven ASCA observations (spanning an entire orbital period of the X-ray source) in the energy range 0.6–10 keV. From these observations we extracted 10 spectra corresponding to different orbital phases. The light curve shows large variability at the orbital phase interval 0–0.2. At phases 0.3–0.6 the light curve is constant, and at phases 0.78–0.89 the count rate decreases.

The equivalent hydrogen absorption column,  $N_{\rm H}$ , derived from the best-fit model to these spectra is  $\sim (1.6-1.7) \times 10^{22}$ 

cm<sup>-2</sup>, in agreement with previous observations (Brandt et al. 1996; Iaria et al. 2001). For a distance to the source of 5.5 kpc, the visual extinction in the direction of Cir X-1 is  $A_v = 5.8 \pm 2.0$  mag (Hakkila et al. 1997). Using the observed correlation between visual extinction and absorption column (Predehl & Schmitt 1995), we find that the expected hydrogen column for Cir X-1 is  $N_{\rm H} = (1.38 \pm 0.02) \times 10^{22}$  cm<sup>-2</sup>. It is slightly smaller than the value obtained from the fit, probably because of the presence of obscuring matter close to the X-ray source. The small fluctuations of the measured Galactic absorption along the orbital phase, which seem to be statistically significant for the intervals A3 and A4 (see Table 3), can be caused by fluctuations in the density (and/or in the ionization level) of this excess of matter around the system.

We fitted the continuum using a Comptonization model. The values of the seed photon and electron temperatures with respect to the orbital phase are plotted in Figure 2 (top and middle panels, respectively). In addition, the spectra A1, F, and G require a partial covering component to fit an iron edge at 7.6–7.9 keV. An absorption edge from ionized iron is present in spectra A4, B, C, and E. In spectrum D the addition of this component is not statistically significant, and we find only an upper limit for its optical depth. The unabsorbed flux, extrapolated in the 0.1–100 keV band, is reported in Figure 3. In this figure we marked the corresponding Eddington flux for a neutron star of 1.4  $M_{\odot}$  at a distance of 5.5 kpc. The flux seems to be super-Eddington at the orbital phases 0–0.2 and 0.95–1 (near the periastron phase).

For each spectrum we calculated the radius,  $R_{\rm w}$ , of the seed photon Wien spectrum using the parameters reported in Tables 3 and 4. Assuming a spherical geometry, this

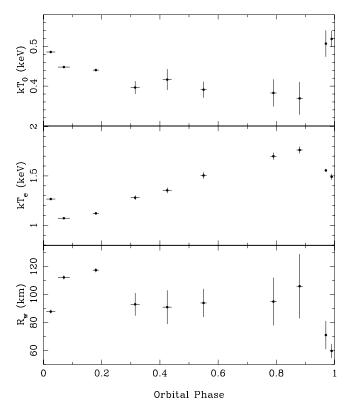


FIG. 2.—Best-fit values of the seed photon temperature (*top*), electron temperature (*middle*), and radius of the seed photons (*bottom*) vs. the orbital phase of Cir X-1.

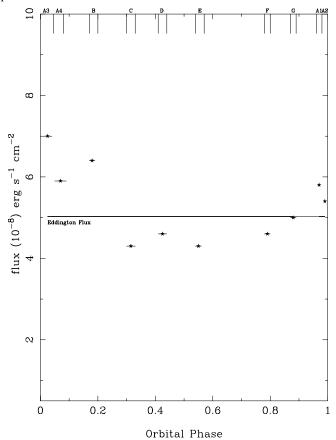


Fig. 3.—Unabsorbed flux of Cir X-1 extrapolated in the 0.1–100 keV band. We mark with a solid line the flux of  $\sim 5 \times 10^{-8}$  ergs s $^{-1}$  cm $^{-2}$ , which is the Eddington flux for a neutron star with a mass of 1.4  $M_{\odot}$  at a distance of 5.5 kpc.

radius can be expressed as  $R_{\rm W} = 3 \times 10^4 D[f_{\rm bol}/$  $(1+y)^{1/2}/(kT_0)^2$  km (in 't Zand et al. 1999), where D is the distance to the source in kiloparsecs,  $f_{bol}$  is the unabsorbed flux of the Comptonization spectrum in units of ergs cm<sup>-2</sup>  $s^{-1}$ ,  $kT_0$  is the seed photon temperature in units of keV, and  $y = 4kT_e \tau^2/m_e c^2$  is the relative energy gain due to the Comptonization. The obtained radii, which are reported in Tables 3 and 4, are in the range between 60 and 120 km. For the sake of clarity  $R_{\mathbf{w}}$  is also plotted versus the orbital phase in Figure 2 (bottom). Following Iaria et al. (2001), we interpret this radius as the inner radius of the disk. Tennant (1987), using EXOSAT data, and Shirey et al. (1996), using RXTE data, observed the presence of a QPO at frequencies between 100 and 200 Hz in Cir X-1. This QPO has been tentatively identified with the lower kilohertz QPO based on the observed correlations among the QPO frequencies in neutron star LMXBs and black hole binary systems (Psaltis, Belloni, & van der Klis 1999), although the interpretation of this feature needs to be confirmed. However, we observe that, assuming that the frequencies of this QPO are related to the Keplerian velocity of the plasma in the accretion disk, we can deduce that the corresponding radii are between 60 and 120 km, similar to the obtained radius of the seed photon-emitting region. Note also that the other luminous low-mass X-ray binaries (LMXBs) of the Z class show a radius of the seed photon-emitting region much closer to the neutron star radius as compared with Cir X-1 (see Di Salvo et al. 2000, 2001), and, accordingly, these Z sources present QPOs at kilohertz frequencies in their power spectra. Note, however, that interpreting the seed photon radius as the inner radius of the disk would imply a quite high accretion rate through the disk of  $\sim 3 \times 10^{18}$  g  $s^{-1}$ , i.e.,  $\sim 3$  times the Eddington accretion rate, for  $R_{\rm W} =$ 120 km and  $kT_0 = 0.4 \text{ keV}$ .

A possible explanation for the large seed photon radius in Cir X-1 is the presence of a relatively large magnetic field: we obtain a magnetic field strength in Cir X-1 of  $\sim 10^{10}$  G, assuming that the measured seed photon radius is the magnetospheric radius. This strength is 1 order of magnitude higher than the supposed magnetic field for LMXBs of the Z class. Moreover, the interpretation of  $R_{\rm W}$  as the magnetospheric radius would imply lower values of  $R_{\rm W}$  at higher flux levels, which is not observed (see Fig. 3), although the error bars are large, especially at phase intervals between 0.3 and 0.9.

Another possible explanation for the large value of the seed photon radius is that the inner region of the disk is either not directly visible, because of the presence of optically thick material in the central part of the system, such as the optically thick corona that probably produces the Comptonization spectrum, or absent, because, for instance, its matter is expelled in a jet or wind. We observe that the seed photon radius seems to increase during the flaring activity at the orbital phase interval between 0 and 0.2. We could suppose that because of the high (probably super-Eddington) accretion rate, a shock is produced in the inner region of the system, pushing the accreting matter toward the external regions. A similar scenario was proposed by Haynes, Lerche, & Murdin (1980), who explained the observed radio flares at the periastron as coming from a shock front formed by the super-Eddington accretion. Also, since Cir X-1 is thought to be observed at a high inclination (Brandt et al. 1996), it is possible that the optically thick material at the shock intercepts and reprocesses the radiation from the inner regions, which cannot therefore be directly observed.

The Comptonized spectrum could originate in an accretion disk corona (ADC) that could be formed by evaporation of the outer layers of the disk illuminated by the emission of the central object (White & Holt 1982). The radius of the corona can be written as  $R_{\rm cor} \simeq$  $(M_{\rm NS}/M_{\odot})T_7^{-1}$   $R_{\odot}$  (White & Holt 1982), where  $M_{\rm NS}$  is the mass of the compact object,  $M_{\odot}$  and  $R_{\odot}$  are the mass and radius of the Sun, respectively, and  $T_7$  is the ADC temperature in units of  $10^7$  K. Under this hypothesis, using the values reported in Tables 3 and 4, we find that the radius of the ADC,  $R_{cor}$ , varies along the orbit in the interval (4.8–  $7.8) \times 10^5$  km. We can infer the density of the ADC using the relation  $\tau = \sigma_T N_e R_{cor}$ , where  $\tau$  is the optical depth obtained from the fit,  $\sigma_T$  is the Thomson cross section,  $N_e$  is the number of particles per unit volume, and  $R_{cor}$  is the ADC radius calculated above. Note that we are considering  $N_e$  constant along the radius of the corona, which is a rough approximation. Under this hypothesis  $N_e$  varies in the range (3.1–6.3)  $\times$  10<sup>14</sup> cm<sup>-3</sup>. These are typical values of density for an ADC (Vrtilek, Soker, & Raymond 1993).

We observe that the electron temperature increases in the orbital phase interval 0.2–0.9, while it decreases in 0.9–1 and 0–0.1. This behavior can be a result of the fact that at orbital phase 0.9, the accretion rate increases, and consequently the inner temperature of the accretion disk increases (as is seen in Fig. 2, top). The injection of more soft photons in the corona enhances the Compton cooling, and the electron temperature decreases. In the orbital interval 0–0.2 the radiation pressure moves the shock to  $\sim$  120 km, and the seed photon temperature decreases, as does the electron temperature. After the injection of soft photons decreases, at orbital interval 0.2–0.9, the cooling of the corona becomes less efficient, and the electron temperature increases.

An iron emission line at energies 6.6–6.8 keV is present in some spectra (A2, A3, A4, C, D, and E), corresponding to emission from Fe xxIII-Fe xxv. The equivalent width of the line is  $\sim 30-70$  eV. We have investigated the hypothesis that this emission line could be produced by reprocessing of X-rays coming from the corona or the inner part of the system by the disk surface (e.g., Brandt & Matt 1994). If Cir X-1 is observed at high inclination (as suggested by Brandt et al. 1996), an iron emission line at  $\sim 6.7$  keV could be produced by the mechanism described above, but the corresponding equivalent width should be  $\sim 20$  eV and the width of the line,  $\sigma_{Fe}$ , should be between 0.6 and 0.8 keV (see Figs. 2, 3, and 4 in Brandt & Matt 1994). The predicted equivalent width seems too low to explain the observed line in Cir X-1. Therefore, in agreement with the Chandra results (Brandt & Schulz 2000), we will consider in the following that the iron emission line is produced in a outflow of ionized matter from the accretion disk (see 4.1).

# 4.1. The Scenario in Cir X-1

In this section we summarize our interpretation of the spectral evolution of Cir X-1 along the orbit based on the results from the analysis described above as well as the *BeppoSAX* results (Iaria et al. 2001), the *Chandra* results (Brandt & Schulz 2000), and the detection in IR and optical bands of emission lines along the orbital period of the source (Johnston et al. 1999).

The broader component of the  $H\alpha$  emission line observed

along the whole orbit of the source can be interpreted as being produced in an outflow of matter with a velocity of  $\sim 2000$  km s<sup>-1</sup> (Johnston et al. 1999). This detection gives us the information that an outflow of matter from the compact system is present in Cir X-1. The lack of the red wing of the line is associated with an optically thick outflow. The Chandra satellite observed the presence of discrete features with P Cygni profiles near the periastron (phase  $\sim$ 0.99) in the X-ray band (Brandt & Schulz 2000). The inferred velocity of the outflow is again  $\sim 2000 \text{ km s}^{-1}$ , in agreement with the results of the IR observations. Moreover, the fact that P Cygni profiles are observed for Fe xxiv and other highly ionized elements suggests that the matter in the outflow at the periastron phase is highly ionized. Iaria et al. (2001) observed near the periastron (phase  $\sim 0.11$ ) the presence of an absorption edge at energy ~8.7 keV corresponding to highly ionized iron. Brandt & Schulz (2000) argue that the absorption edge could be associated with the outflow, probably consisting of a thermally driven wind formed by the X-rays from the inner region that heats the disk surface. It is not straightforward to infer the geometry (radial or vertical) of the outflow from these data. However, we can see that the model of thermally driven wind proposed by Begelman, McKee, & Shields (1983) could explain the observed outflow. In this model the outflow is near the disk surface and mainly in the direction of the observer (Begelman et al. 1983; Begelman & McKee 1983). This seems reasonable in the case of Cir X-1, given that Brandt et al. (1996) argued that Cir X-1 is almost edge-on and that the P Cygni profiles (to date the only ones observed in an LMXB) indicate that we are observing the approaching part of the outflow. This geometry could also explain the large optical depth of the iron absorption edge ( $\tau \sim 1$ ; Iaria et al. 2001). However, the model of thermally driven wind does not take into account the radiation pressure and is valid for luminosities of a few percent of the Eddington luminosity or less (Begelman et al. 1983), while the radiation pressure could be significant in Cir X-1 because of the high luminosity of the source, especially near the periastron.

The study of Cir X-1 along the entire orbit allows us to describe the evolution of the iron absorption edge and emission line present in the spectra with a scenario in which an outflow from the system is almost always present but in which its physical conditions change as a function of the accretion rate along the orbital period. We distinguish three states of the source along the orbit:

- 1. A super-Eddington state at phases 0.99–1 and 0–0.20, when the outflow of highly ionized matter (and probably a shock too) is formed;
- 2. A quiet state between 0.3 and 0.7, when the source has a sub-Eddington luminosity and the outflow is weaker; and
- 3. A partial covering state between 0.77 and 0.95, when the atmosphere of the companion star and/or the accreting matter from the companion, which probably forms a bulge in the outer disk, partially cover the emission from the compact object.

# 4.1.1. The Super-Eddington State: Presence of an Outflow of Highly Ionized Matter

The spectra A2, A3, A4, and B belong to the same state of the source corresponding to the phase interval around the

periastron, 0.99-1 and 0-0.2. In these spectra there is no evidence of partial covering, which suggests the absence of neutral matter around the system (contrary to what is observed at previous orbital phases, between 0.78 and 0.96; see § 4.1.3). The flux is super-Eddington for each spectrum for the assumed distance and with the hypothesis that the emission from the source is mainly isotropic. In this state a shock probably forms in the inner region of the system, and radio and X-ray flares might be associated with the shock front (Haynes et al. 1980). The P Cygni profiles observed by Brandt & Schulz (2000) could be produced by the high luminosity (and then the high radiation pressure) that sweeps away and ionizes the accreting matter around the system. In spectra A2 and A3 we do not detect the absorption edge, but an iron emission line is present at energy  $\sim 6.6 \text{ keV}$  (produced by Fe xxIII; Turner et al. 1992) and ~6.7 keV (Fe xxiv-Fe xxv), respectively, implying a gradual increase of the ionization level in the outflow. The equivalent width of the iron energy line at  $\sim 6.6$  keV is  $\sim 30$ eV, which is smaller than the equivalent width of the iron emission line in the other spectra, probably because the fluorescence yield associated with Fe xxIII is smaller than that associated with Fe xxiv and Fe xxv (Turner et al. 1992). Under the hypothesis that the iron emission line is associated with the outflow, we deduce that during intervals A2 and A3, the matter in the outflow is also highly ionized. We argue that the outflow has a low density at these orbital phases because the absorption edge is not observed (the corresponding equivalent hydrogen column is lower than  $10^{23}$  cm<sup>-2</sup>). The presence of the H $\alpha$  line, detected at these phases by Johnston et al. (1999), suggests that the matter of the outflow is either photoionized or heated by a nonthermal emission. In fact, if the matter in the outflow were heated by a thermal emission, we should not observe an  $H\alpha$ emission because recombination to neutral hydrogen should not be possible.

In spectra A4 and B (the orbital phase interval 0.05–0.19), an absorption edge is present. The energy of the edge is 8.46 and 8.71 keV, respectively. These energies are compatible with iron ionization levels of Fe xxIII-Fe xxv (Turner et al. 1992). The best-fit value for the optical depth  $\tau_{\rm edge}$ , considering the photoionization cross section for the K shell of Fe XXIII (Krolik & Kallman 1987) and assuming cosmic abundance of iron, corresponds to a hydrogen column density of  $\sim 6 \times 10^{23}$  and  $\sim 7 \times 10^{23}$  cm<sup>-2</sup> for A4 and B, respectively, in agreement with the results reported by Iaria et al. (2001). The iron ionization level is similar to that in spectra A2 and A3, and the presence of the edge could be explained by an increase of the density and/or optical depth of the outflow. The iron emission line is still observed in spectrum A4 (together with the absorption edge), but it is not detected is spectrum B.

## 4.1.2. The Quiet State

The spectra C, D, and E, corresponding to the orbital phase interval 0.3–0.6, show a sub-Eddington flux: the light curve is quite constant at  $\sim 300$  counts s<sup>-1</sup>, and the hardness ratio increases from  $\sim 0.75$  up to 0.9. The seed photon radius is constant at  $\sim 90$  km, and the seed photon temperature is constant at  $\sim 0.4$  keV, while the electron temperature increases from 1.2 up to 1.5 keV. In these spectra an absorption edge is present at  $\sim 8.3$  keV, with optical depth decreasing from 0.12 to 0.06. The energy of  $\sim 8.3$  keV indicates that the matter is less ionized, and the low values

of the optical depth indicate that the absorption column decreases. The equivalent hydrogen column goes from  $\sim 2.6 \times 10^{23}$  down to  $\sim 10^{23}$  cm<sup>-2</sup>. An iron emission line is also present, the energy of which is stable at  $\sim 6.7$  keV. This indicates that the outflow is still present, although it is now probably much weaker.

# 4.1.3. The Partial Covering State: Absorption from Neutral Matter Coming from the Companion Star

Cir X-1 has a highly eccentric orbit ( $e \sim 0.9$ ; Murdin et al. 1980; Tauris et al. 1999). It is possible that, for the geometry of the system (see, e.g., Fig. 4 in Johnston et al. 1999) near the periastron, the neutron star is occulted by the outer layers of the companion star atmosphere. Also, the high eccentricity of the orbit might produce large tidal interactions at these phases, which expand and/or deform the stream of the accreting matter, possibly forming a bulge in the outer accretion disk. The excess of neutral matter modifies the observed emission of the X-ray source, producing a partial covering of the energy spectrum of the source (see also Inoue 1989). The partial covering component is detected in spectra A1, F, and G, corresponding to the phase interval between 0.78 and 0.97. In this state the (ionized) iron absorption edge and emission line are not detected. At orbital phase  $\sim 0.78$  the hydrogen column, inferred from the partial covering, is  $\sim 6.9 \times 10^{23}$  cm<sup>-2</sup>, and it increases up to  $\sim 11 \times 10^{23}$  cm<sup>-2</sup> at the orbital phase  $\sim 0.89$ . This is probably caused by the approach of the X-ray source to the companion star. At 0.95 the hydrogen column decreases to  $\sim 1 \times 10^{23}$  cm<sup>-2</sup>, and the partial covering component disappears at the following orbital phases. The decrease of the hydrogen column can be caused by the increase of the accretion rate to super-Eddington values, which photoionizes the surrounding neutral matter. In fact, the X-ray flux increases from spectrum F to spectrum G (see Fig. 3), indicating that the accretion rate increases at these phases.

#### 4.2. Comparison with Other Luminous LMXBs

Recently, several Z sources were analyzed using a broadband (0.1-200 keV) energy range (e.g., GX 17+2, Di Salvo et al. 2000; GX 349+2, Di Salvo et al. 2001). Their spectra show an absorption edge associated with highly ionized matter, as it is observed in Cir X-1. The hydrogen column associated with the absorption edge in these Z sources is less than  $1 \times 10^{23}$  cm<sup>-2</sup>, and the equivalent widths of the iron emission lines present in these spectra are  $\sim 40-70$  eV. According to Vrtilek et al. (1993), who suppose that emission lines are produced in a photoionized ADC, these equivalent widths could be expected in sources with a low inclination angle. The phenomenon of the outflow from the accretion disk connected to Eddington sources is partially confirmed by the detection, in the IR band, of lines with P Cygni profiles in Sco X-1 and GX 13+1 (Bandyopadhyay et al. 1999). Because the outflow of ionized matter should be mostly along the disk surface, the absorption edge should be more evident in sources with high inclination. Therefore, the small values of the optical depth of the absorption edge in GX 17+2 and GX 349+2 could be associated with low inclinations. In this case, the absorption edge might be considered an indicator of the inclination angle of the source.

## 5. CONCLUSIONS

We have analyzed observations of Cir X-1 from the ASCA archive performed in 1998 March and corresponding

328 IARIA ET AL.

to a whole orbital period. Cir X-1 is most probably a highinclination source, and this might explain why we do not observe the blackbody emission of the neutron star or inner accretion disk. We observe a Comptonized component probably coming from an ADC. We find that the optical depth of the Comptonizing region is  $\sim 20$ , the seed photon temperature ranges from 0.4 to 0.5 keV, and the electron temperature increases from 1 keV at phase 0.05 up to 1.8 keV at phase 0.9. The radius of the seed photons is around 90 km. This could be explained either by a magnetic field of 10<sup>10</sup> G or, more probably, by the presence of optically thick material in the inner part of the system that hides the innermost regions. During the observations, which span an entire orbital period of the X-ray source, it is possible to distinguish three states of the source: a high accretion rate (probably super-Eddington) state, where X-ray flares are present near the periastron; a quiet state, where the system accretes at a sub-Eddington rate at orbital phases from 0.3 to  $\sim 0.7$ ; and a partial covering state at orbital phases 0.78– 0.97. The first state is characterized by the presence of a prominent iron absorption edge, probably produced in an outflow of highly ionized matter. The matter is swept away and photoionized by the high luminosity of the X-ray source in this state. The second state shows an absorption edge of less ionized iron with an equivalent hydrogen column smaller than  $10^{23}$  cm<sup>-2</sup>; the outflow is probably still present in this state, although much weaker. The third state is characterized by the presence of partial covering, explained as being the result of absorption by the atmosphere of the companion star and/or by the accreting matter from the companion, which, at these orbital phases, can fall in the line of sight between the X-ray source and the observer.

This work was supported by the Italian Space Agency and by the Ministero della Ricerca Scientifica e Tecnologica. This research has made use of data obtained through the High Energy Astrophysics Science Archive Research Center Online Service, provided by the NASA/Goddard Space Flight Center.

#### REFERENCES

Bandyopadhyay, R. M., Shahbaz, T., Charles, P. A., & Naylor, T. 1999, MNRAS, 306, 417 Begelman, M. C., & McKee, C. F. 1983, ApJ, 271, 89
Begelman, M. C., McKee, C. F., & Shields, G. A. 1983, ApJ, 271, 70
Brandt, W. N., Fabian, A. C., Dotani, T., Nagase, F., Inoue, H., Kotani, T., & Segawa, Y. 1996, MNRAS, 283, 1071 Brandt, W. M., & Matt, G. 1994, MNRAS, 268, 1051 Brandt, W. N., & Schulz, N. S. 2000, ApJ, 544, L123 Case, G. L., & Bhattacharya, D. 1998, ApJ, 504, 761 Clark, D. H., Parkinson, J. H., & Caswell, J. L. 1975, Nature, 254, 674 Di Salvo, T., Robba, N. R., Iaria, R., Stella, L., Burden, L., & Israel, G. L. 2001, ApJ, 554, 49 Di Salvo, T., et al. 2000, ApJ, 544, L119 Hakkila, J., Myers, J. M., Stidham, B. J., & Hartmann, D. H. 1997, AJ, 114, Haynes, R. F., Lerche, I., & Murdin, P. 1980, A&A, 87, 299 Iaria, R., Burderi, L., Di Salvo, T., La Barbera, A., & Robba, N. R. 2001, ApJ, 547, 412 Inoue, H. 1989, in 23d ESLAB Symp., Two Topics in X-Ray Astronomy, ed. N. E. White, J. Hunt, & B. Battrick (Paris: ESA), 109 in 't Zand, J. J. M., et al. 1999, A&A, 345, 100 Johnston, H. M., Fender, R., & Wu, K. 1999, MNRAS, 308, 415 Krolik, J. H., & Kallman, T. R. 1987, ApJ, 320, L5

Makishima, K., et al. 1996, PASJ, 48, 171 Mitsuda, K., et al. 1984, PASJ, 36, 741 Murdin, P., Jauncey, D. L., Haynes, R. F., Lerche, I., Nicolson, G. D., Holt, S. S., & Kaluzienski, L. J. 1980, A&A, 87, 292 Ohashi, T., et al. 1996, PASJ, 48, 157 Predehl, P., & Schmitt, J. H. M. M. 1995, A&A, 293, 889 Psaltis, D., Belloni, T., & van der Klis, M. 1999, ApJ, 520, 262 Shirey, R. E., Bradt, H. V., Levine, A. M., & Morgan, E. H. 1996, ApJ, 469, . 1999, ApJ, 517, 472 Stewart, R. T., Nelson, G. J., Penninx, W., Kitamoto, S., Miyamoto, S., & Nicolson, G. D. 1991, MNRAS, 253, 212 Tanaka, Y., Inoue, H., & Holt, S. S. 1994, PASJ, 46, L37 Tauris, T. M., Fender, R. P., van den Heuvel, E. P. J., Johnston, H. M., & Wu, K. 1999, MNRAS, 310, 1165 Tennant, A. F. 1987, MNRAS, 226, 971 Titarchuk, L. 1994, ApJ, 434, 570 Toor, A. 1977, ApJ, 215, L57 Turner, T. J., Done, C., Mushotzky, R., & Madejski, G. 1992, ApJ, 391, 102 Vrtilek, S. D., Soker, N., & Raymond, J. C. 1993, ApJ, 404, 696 White, N. E., & Holt, S. S. 1982, ApJ, 257, 318